Available online at www.sciencedirect.com
ScienceDirect
Ultramicroscopy 107 (2007) 969–979
ultramicroscopy
www.elsevier.com/locate/ultramic

Hierarchical roughness optimization for biomimetic superhydrophobic surfaces

Michael Nosonovsky[a], Bharat Bhushan[b,*]

[a]National Institute of Standards and Technology, Gaithersburg, MD 20899-8520, USA
[b]Nanotribology Laboratory for Information Storage and MEMS/NEMS, 201 W. 19th Avenue, The Ohio State University, Columbus, OH 43210-1142, USA

Abstract

Superhydrophobic surfaces should have high contact angles (CA) with water and low contact angle hysteresis (CAH). High CA may be achieved by increasing surface roughness, while in order to have low CAH, superhydrophobic surfaces should be able to form a stable composite interface with air pockets between solid and liquid. Capillary waves, nanodroplets condensation, hydrophilic spots due to chemical surface inhomogeneity, and liquid pressure can destroy the composite interface. These destabilizing factors have different characteristic length scales, so a hierarchical roughness is required to resist them. It is shown that convex rather than concave profile enhances stability, so nanoscale convex bumps should be superimposed over microasperities, in order to pin the liquid–air interface. In addition, the nanoroughness is required to support nanodroplets. The ability of the interface to support high pressure requires high asperity density and size, so it is in conflict with the requirement of low fractional solid–liquid contact area for low CAH and slip length. The new parameter, spacing factor for asperities, is proposed, and requirements for optimum design, which combines conflicting conditions, are formulated and discussed. Remarkably, biological superhydrophobic surfaces satisfy these requirements.

PACS: 61.30.Hn; 68.08.−p; 68.08.Bc

Keywords: Surface phenomena; Liquid–solid interfaces; Wetting

1. Introduction

The rapid advances in *Nanotechnology* since 1980s, including such applications as micro/nanoelectromechanical systems (MEMS/NEMS), have stimulated development of new materials and design of surfaces, which should meet new sets of requirements [1,2]. In MEMS/NEMS, surface-to-volume ratio grows with miniaturization and surface phenomena dominate. One of the crucial surface properties for materials in micro/nanoscale applications is water repellency, non-wetting or hydrophobicity. It is also usually desirable to reduce wetting and increase liquid slip in liquid flow applications. Wetting is characterized by the contact angle (CA), which is defined as the measurable angle, which a liquid makes with a solid. The CA depends on several factors, such as roughness and the manner of surface preparation, and its cleanliness [3,4]. If the liquid wets the surface (referred to as wetting liquid or hydrophilic surface), the value of the CA is $0 \leqslant \theta \leqslant 90^\circ$, whereas if the liquid does not wet the surface (referred to as non-wetting liquid or hydrophobic surface), the value of the CA is $90^\circ \leqslant \theta \leqslant 180^\circ$. The term hydrophobic/philic, which was originally applied only to water, is sometimes used to describe the contact of a solid surface with any liquid. Surfaces with the CA between 150° and 180° are called superhydrophobic. Superhydrophobic surfaces also have very low water contact angle hysteresis (CAH). The CAH is the difference between the advancing and receding CAs. If additional liquid is added to a sessile drop, the contact line advances and each time motion ceases, the drop exhibits an advancing CA. Alternatively, if liquid is removed from the drop, the CA decreases to a receding value before the contact retreats. For a droplet, moving along the solid surface, the CA at the front of the droplet (advancing CA) is greater than that at the back of the

*Corresponding author. Tel.: +1 614 292 0651; fax: +1 614 292 0325.
E-mail address: Bhushan.2@osu.edu (B. Bhushan).

0304-3991/$ - see front matter © 2007 Elsevier B.V. All rights reserved.
doi:10.1016/j.ultramic.2007.04.011

droplet (receding CA), due to roughness and surface heterogeneity, resulting in the CAH.

One of the ways to increase the hydrophobic or hydrophilic properties of the surface is to increase surface roughness; so roughness-induced hydrophobicity has become a subject of extensive investigation. Wenzel [5] found that the CA of a liquid with a rough surface is different from that with a smooth surface. Cassie and Baxter [6] showed that air (or gas) pockets may be trapped in the cavities of a rough surface, resulting in a composite solid–liquid–air interface, as opposed to the homogeneous solid–liquid interface. Johnson and Dettre [7] showed that the homogeneous and composite interfaces correspond to the two equilibrium states of a droplet. Bico et al. [8], Marmur [9,10], Lafuma and Quėrė [11], Patankar [12,13], He et al. [14], Li and Amirfazli [15] and other authors have recently investigated metastability of artificial superhydrophobic surfaces and showed that whether the interface is homogeneous or composite may depend on several factors, such as surface geometry and history of the system (in particular, whether the liquid was applied from the top or from the bottom). Extrand [16] pointed out that whether the interface is homogeneous or composite depends on droplet size, due to the gravity. It was suggested also that the so-called two-tiered (or double) roughness, composed by superposition of two roughness patterns at different length scale [17–19], and fractal roughness [20] may lead to superhydrophobicity. Herminghaus [17] showed that certain self-affine profiles may result in superhydrophobic surfaces even for wetting liquids, in the case the local equilibrium condition for the triple line (line of contact between solid, liquid and air) is satisfied. Nosonovsky and Bhushan [21,22] pointed out that such configurations, although formally possible, are likely to be unstable. Nosonovsky and Bhushan [22,23] proposed a stochastic model for wetting of rough surfaces with a certain probability associated with every equilibrium state. According to their model, the overall CA with a two-dimensional rough profile is calculated by assuming that the parts of the interface are homogeneous, while other parts form a composite interface. The probability-based concept is consistent with the experimental data [11], which suggests that transition between the composite and homogeneous interfaces is gradual, rather than instant.

It has been demonstrated experimentally that roughness indeed changes CA [20,24–27]; superhydrophobicity has also been studied by simulation using the mean-field theory of liquid droplets [28,29]. A number of works on liquid flow in superhydrophobic channels also appeared recently [29,30].

Study and simulation of biological objects with desired properties is referred to as "biomimetics," which comes from a Greek word "biomimesis" meaning to mimic life. Some natural surfaces, including leaves of water-repellent plants, such as the lotus (*Nelumba nucifera*), legs of insects, such as the water strider (*Gerris remigis*), and butterfly wings, etc., are known to be very hydrophobic due to roughness of their surface [31–35]. This phenomenon, along with self-cleaning abilities of very hydrophobic surfaces is called in the literature "lotus effect" [31]. There is a significant literature about the lotus effect, and numerous attempts to produce artificial biomimetic roughness-induced hydrophobic surfaces have been made [13,19,24,36–38], but many details of the mechanism of roughness-induced non-wetting are still not well understood. In particular, it is not clear why lotus leaf and other natural hydrophobic surfaces have a multiscale (or hierarchical) roughness structure, that is, nanoscale bumps superimposed over microscale asperities. As far as realization of strongly water-repellent artificial surfaces is concerned, they can be constructed by chemically treating surfaces with low-surface-energy substances, such as polytetrafluoroethylene, silicon, or wax, or by fabricating extremely rough hydrophobic surfaces directly [14,20,38,39]. Sun et al. [19] studied an artificial poly(dimethylsiloxane) (PDMS) replica of a lotus leaf surface and found the water CA of 160° for the rough surface, whereas for the smooth PDMS surface it is about 105°.

From the design viewpoint, it is important to investigate optimum roughness distribution for superhydrophobicity. Nosonovsky and Bhushan [21] formulated requirements, which should be satisfied by rough surfaces, optimized for CA and meniscus force. Nosonovsky and Bhushan [40,41] also showed that in order to minimize CAH, a stable composite interface should exist. Since destabilizing factors for the composite interface have different length scales, in order to maintain stability of the interface, roughness should be multiscale or hierarchical. In this paper, we formulate optimization criteria for hierarchical roughness for maximum CA and minimum CAH and apply it for both liquid droplets and liquid flow and compare them with the available experimental data of biological and artificial superhydrophobic surfaces.

2. CA and CAH analysis for a liquid in contact with a rough surface

In this section, we examine dependence of CA and CAH upon surface roughness. High CA indicates that liquid is repelled by the solid surface; whereas low CAH indicates that a liquid has low adhesion to a solid and thus can flow easily with low-energy dissipation. Therefore, superhydrophobic surfaces should have both high CA and low CAH. Liquid may form either homogeneous interface with a solid, or a composite interface with air pockets trapped between the solid and liquid. The composite interface may be destabilized, if air pockets are pushed away from the interface. Multiple equilibrium states are possible, which correspond to homogeneous interface, composite interface, or mixed interface with some air pockets pushed away from the interface while others are still sitting at the interface. We investigate CA and CAH under these varieties of conditions and identify multiscale factors, which affect both CA and CAH.

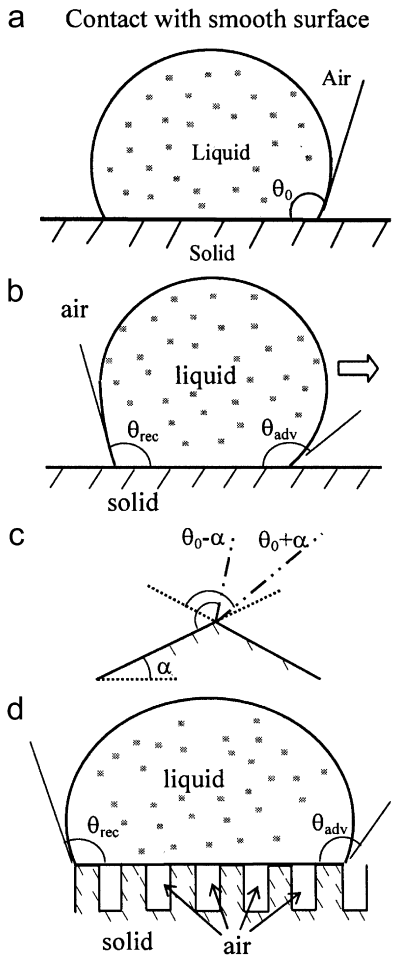

Fig. 1. Liquid droplet in contact with (a) smooth profile (the value of CA is θ_0), (b) rough profile (the values of advancing and receding CA are θ_{adv} and θ_{rec}), (c) sharp edge (the values of CA may vary between $\theta_0-\alpha$ and $\theta_0+\alpha$), and (d) rough profile with composite interface.

2.1. Homogeneous interface

If a droplet of liquid is placed on a solid surface, the solid–air and liquid–air interfaces come together under the static CA, θ_0 (Fig. 1(a)). The value of θ_0 can be determined from the condition of the total free energy of the system being minimized [3,4] and is given by the so-called Young–Dupré equation for the CA:

$$\cos\theta_0 = \frac{\gamma_{SA}-\gamma_{SL}}{\gamma_{LA}} = \frac{W}{\gamma_{LA}} - 1, \tag{1}$$

where γ_{SL}, γ_{SA} and γ_{LA} are solid–liquid, solid–air, and liquid–air interface free energies and W is the work of adhesion. Note that although the term "air" is used throughout this paper, the analysis does not change in the case of another gas, such as a liquid vapor.

For micro/nanoscale droplets, the value of the CA may be different than for macroscale droplets. The effect of line tension is believed to be responsible for that, since the energy of molecules in the vicinity of the triple line is different from that in the bulk or at the surface. However, this effect is significant only at nanometer range [42]. Checco et al. [43] showed that the atomic force microscopy data on scale dependence of the CA for nano/microsized droplets may rather be explained by the effect of surface heterogeneity, assuming that tiny droplets first appear at the most wettable spots.

For a rough solid surface, which consists of asperities and valleys, with a typical size of roughness details smaller than the size of the droplet, the CA was calculated by Wenzel [5]

$$\cos\theta = R_f \cos\theta_0, \tag{2}$$

where θ is the CA for rough surface, R_f is a roughness factor defined as a ratio of the solid–liquid area A_{SL} to its projection on a flat plane, A_F

$$R_f = \frac{A_{SL}}{A_F}. \tag{3}$$

According to Eq. (2), which relates CA to roughness, if the liquid wets a flat surface ($\cos\theta_0>0$), it will wet also the rough surface with a CA of $\theta<\theta_0$, since $A_{SL}/A_F>1$. Furthermore, for non-wetting liquids ($\cos\theta_0<0$), the CA with a rough surface will be greater than that with the flat surface, $\theta>\theta_0$.

Another important characteristic of a solid–liquid interface is the CAH, which may exist due to several reasons, including surface roughness and heterogeneity Fig. 1(b). There is no simple expression for the CAH as a function of roughness; however, certain conclusions about the relation of the CAH to roughness can be made. Fig. 1(c) shows a droplet, flowing along a solid surface with sharp edges with the liquid–air interface pinned by a sharp edge. At the edge point, the CA is not defined and can have any value between the values corresponding to the contact with the horizontal and inclined surfaces. As it is observed from Fig. 1(c), because of the change of the surface slope (α) at the edge, the value of the CA at the front of the droplet (maximum advancing CA or $\theta_{adv}=\theta_0+\alpha$) is greater than θ_0, whereas the value of the CA at the back of the droplet (minimum receding CA or $\theta_{rec}=\theta_0-\alpha$) is smaller than θ_0, Thus, CAH at a surface with grooves, Fig. 1(d), is estimated as the change of surface slope, 2α. For a more accurate calculation of the CAH, the height of energy barriers associated with motion of the droplet along a rough surface with a particular profile should be calculated [7]. For a chemically heterogeneous surface, the change of local CA due to heterogeneity has a similar effect as the change of the surface slope [44].

Even liquid in contact with a nominally flat surface has CAH due to a number of reasons, such as micro/nanoscale roughness and inhomogeneity, chemical interactions at the interface, the so-called adhesion hysteresis, the difference ΔW between the energy gained for surfaces coming to contact and the work of adhesion for separating surface [4].

2.2. Composite interface

For a rough surface, a composite solid–liquid–air interface may form air pockets at the valleys between asperities with the flat fractional geometrical area of the solid–liquid and solid–air interfaces under the droplet f_{SL} and $1-f_{SL}$, respectively. Transition to the composite interface increases CA and dramatically decreases solid–liquid contact area, and therefore decreases adhesion of liquid to solid and CAH, allowing the droplet to roll easily along the solid surface [7]. Cassie and Baxter [6] found that for fractional solid–liquid and solid–air interfaces, the CA is given by

$$\cos\theta = R_f f_{SL}\cos\theta_0 - 1 + f_{SL}. \quad (4)$$

Eq. (2) may now be considered a special case of Eq. (4) with $f_{SL}=1$ (no air under the droplet).

Since the work of adhesion is proportional to the contact area between the solid and liquid, for a composite interface, adhesion hysteresis is proportional to the solid–liquid area $\Delta W = f_{SL}R_f\Delta W_0$, where ΔW_0 is adhesion hysteresis for a smooth surface. The adhesion hysteresis is related to the CAH, although it does not uniquely define the later. There are many factors that affect the CAH, including the adhesion hysteresis, surface roughness and heterogeneity. For an exact theoretical calculation of the CAH, a thermodynamic analysis of energy barriers for a moving droplet would be required [7], which is a complicated problem in the case of the three-dimensional geometry. We will assume that the CAH is equal to the term corresponding to the adhesion hysteresis ΔW plus the term corresponding to the effect of surface roughness, H_r. We assume also that Eq. (4), which normally applies to the thermodynamic equilibrium and is valid for the most stable CA, applies also to the effect of the adhesion hysteresis upon the CAH. Using Eq. (4), the difference of cosines of the advancing and receding angles is related to the difference of those for a nominally smooth surface, θ_{adv0} and θ_{rec0}, as

$$\cos\theta_{adv} - \cos\theta_{rec} = \frac{\Delta W}{\gamma_{LA}} = \frac{R_f f_{SL}\Delta W_0}{\gamma_{LA}} = R_f f_{SL}(\cos\theta_{adv0} - \cos\theta_{rec0}) + H_r. \quad (5)$$

Non-dimensional parameter H_r is responsible for the pinning effect of the sharp edges. It may be assumed to be proportional to the density of sharp edges per unit area. In the case of small H_r, it is observed from Eqs. (4),(5) that decreasing $f_{SL}\to 0$ results in increasing CA ($\cos\theta\to -1, \theta\to\pi$) and decreasing CAH ($\cos\theta_{adv}-\cos\theta_{rec}\to 0$). In the limiting case of very small solid–liquid fractional contact area under the droplet, when the CA is large ($\cos\theta\approx -1+(\pi-\theta)^2/2$; $\sin\theta\approx\theta-\pi$) and CAH is small ($\theta_{adv}\approx\theta\approx\theta_{rec}$), Eqs. (4) and (5) are reduced to

$$\pi-\theta = \sqrt{2f_{SL}(R_f\cos\theta_0+1)}, \quad (6)$$

$$\theta_{adv}-\theta_{rec} = f_{SL}R_f\frac{\cos\theta_{a0}-\cos\theta_{r0}}{-\sin\theta} = \sqrt{f_{SL}}R_f\frac{\cos\theta_{r0}-\cos\theta_{a0}}{\sqrt{2(R_f\cos\theta_0+1)}}. \quad (7)$$

For the homogeneous interface, $f_{SL}=1$, whereas for composite interface f_{SL} is a small number. It is observed from Eqs. (4)–(7) that for homogeneous interface, increasing roughness (high R_f) leads to increased CAH (high values of θ_{adv}–θ_{rec}), while for composite interface, small values of f_{SL} provide with both high CA and small CAH. Therefore, composite interface is essential for superhydrophobicity.

The superhydrophobic state, corresponding to composite interface, is likely to exist only for hydrophobic materials, since otherwise it will be energetically profitable for the liquid to spread and fill the valleys. However, it has been reported [11,42] that metastable composite interface was observed experimentally even for hydrophilic materials ($\theta_0<90^\circ$), while the physical mechanism of this effect has not been adequately explained.

2.3. Mixed interface and stochastic model for metastable states

The homogeneous and composite interfaces correspond to two limiting cases of equilibrium with all valleys either filled with liquid or with air pockets. These equilibriums correspond to two local free energy minima E_h and E_c. Which equilibrium is actually realized, depends upon the history of the system (whether the droplet was imposed over the tops of the asperities from above, or the liquid condensed in the valleys) and on vibrational energy of the droplet (whether it is greater than energy barrier separating the equilibrium state). However, in addition to these two limiting cases of equilibrium, there are many intermediate metastable states E_n, for which some valleys are filled with liquid and some still have air pockets, and which correspond to local energy minima E_h. Nosonovsky and Bhushan [22,23] suggested that certain probabilities p_n could be associated with the equilibrium states E_n and proposed a stochastic model to analyze these states. They further assumed that in the case of thermally activated change of equilibrium, p_n is related to E_n, based on the Maxwell–Boltzmann statistical distribution, as

$$p_n = B\exp\left(-\frac{E_n}{kT}\right), \quad (8)$$

where kT is the Boltzmann constant times temperature of the system and B is a proportionality constant. Based on this model, they calculated values of R_f and F_{SL}, and found the values of CA from Eq. (4) in the range between those predicted by the Wenzel equation (Eq. (2)) for the homogeneous interface and Cassie–Baxter equation (Eq. (4)) for the composite interface.

An alternative approach involves various techniques of simulation at molecular scale or mesoscale, such as the

molecular dynamic simulation [45], lattice Boltzmann method, mean-field Boltzmann method [28,29], etc. These studies have provided with values of CA in the range between those predicted by the Wenzel and Cassie–Baxter model.

2.4. Stability of composite interface

As it was shown in the preceding sections (Eq. (5)), the composite interface is important in order for surface to have high CA and, especially, low CAH. An experimental evidence of that was provided by Sun et al. [19]. They produced both a positive and a negative replica of a lotus leaf surface by nanocasting using poly(dimethylsiloxane), which has the CA with water of about 105°. This value is close to the CA of wax, which covers lotus leaves (about 103° as reported by Kamusewitz et al. [46]). The positive and negative replicas have the same roughness factor and thus should produce the same CA in the case of a homogeneous interface, according to Eq. (6); however, the values of surface curvature are opposite. The value of CA for the positive replica was found 160° (close to that of the lotus leaf), while for the negative replica it was only 110°. This result suggests that high CA for lotus leaf is due to the composite, rather than homogeneous interface, and that the sign of surface curvature plays a critical role for formation of the composite interface.

Three factors can destroy the composite interface. First, the capillary waves at the LA interface may destabilize the composite interface (Fig. 2), and their effect is more pronounced for small asperities with height comparable with wave amplitude [21–23].

Second, nanodroplets may condensate and accumulate in the valleys between asperities and eventually destroy the composite interface. Cheng et al. [38] observed condensation of submicron size droplets on a lotus leaf surface and found that droplets tend to condensate at areas adjacent to bumps (i.e., in the valleys) and have CA of less than 90°. This observation showed that droplets condensation in the valleys does not necessary lead to the composite interface and can serve as a further evidence of importance of the composite interface. It also caused a discussion on whether superhydrophobic surfaces are always water repellent [47,48]. When the composite interface is destroyed and space between asperities is filled with water, it is highly unlikely that it will be formed again because transition from homogeneous to composite interface would require large activation energy. Such transition has never been observed [42].

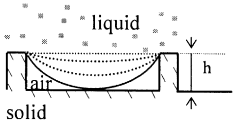

Fig. 2. Destabilization of the composite interface due to increasing amplitude of a liquid–air interface capillary wave. If wave amplitude is high enough so that it touches the valley between asperities, the liquid can fill the valley.

Third, even hydrophobic surfaces are usually not chemically homogeneous and can have hydrophilic spots. It is known from experiments that for droplets of submicron size, the value of the CA is usually smaller than for the droplets at the macroscale [11]. Checco et al. [43] suggested that surface inhomogeneity is responsible, since nanodroplets tend to sit at the highest free surface energy (most hydrophilic) spots and thus have lower CAs. Their phenomenological numerical simulations showed good agreement with experimental data.

To guarantee that the equilibrium provides with a local minimum and not maximum of the total energy, $d^2W>0$, which yields

$$d^2W = d^2A_{SL}\left[\cos\theta_0 - \frac{\gamma_{SA}-\gamma_{SL}}{\gamma_{LA}}\right]\gamma_{SL} + dA_{LA}\,d(\cos\theta) > 0. \tag{9}$$

Using Eq. (9), which is satisfied at the equilibrium, and the fact that $\cos\theta$ decreases monotonically with θ at the domain of our interest, $0<\theta<180°$, yields

$$dA_{SL}\,d\theta_0 < 0. \tag{10}$$

Based on Eq. (10), for the interface to be stable, the value of the CA should decrease when the liquid–air interface advances, whereas for receding liquid the CA should increase (Fig. 3). For a two-dimensional surface, change of angle is equal to the change of slope of the surface, and whether the configuration is stable or not depends on the sign of curvature of the surface. The convex surface (with bumps) leads to a stable interface, whereas concaved surface (with grooves) leads to an unstable interface. Thus, the surface with bumps can actually pin the liquid–air interface even for hydrophilic surface.

We have identified mechanisms, which lead to destabilization of the composite interface, namely, the capillary waves, condensation and accumulation of nanodroplets, and surface inhomogeneity. These mechanisms are scale

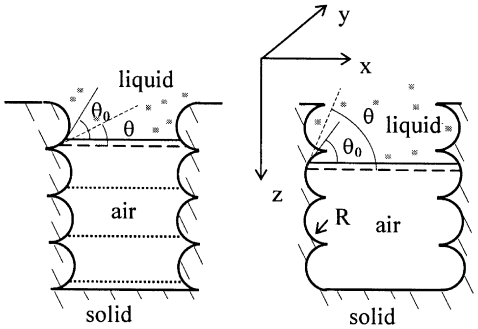

Fig. 3. Schematics of multiscale roughness with small bumps/grooves over large asperities (pillars). The bumps may pin the triple line even in the case of a hydrophilic material ($\theta_0<90°$), because with advancing LA interface, the angle between the solid and the LA interface decreases ($\theta<\theta_0$), while the grooves cannot pin the interface ($\theta>\theta_0$). Thus, bumps lead to stable LA interfaces (multiple positions of stable interface are shown with dotted lines) whereas grooves lead to unstable LA interface.

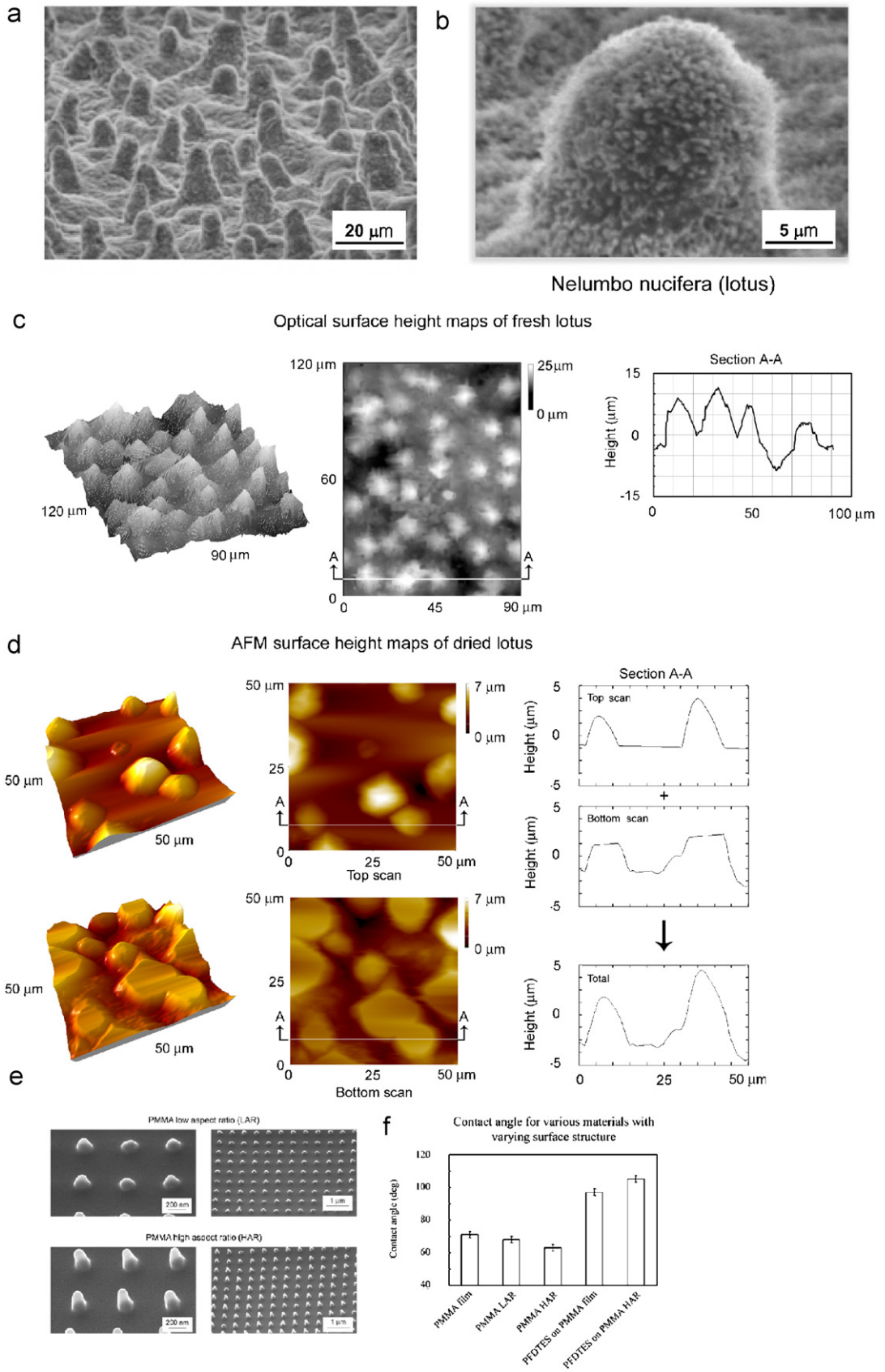
a
20 μm
b
5 μm
Nelumbo nucifera (lotus)
c
Optical surface height maps of fresh lotus
120 μm
90 μm
120 μm
25μm
0 μm
60
A
A
0
0
45
90 μm
Section A-A
15
0
-15
Height (μm)
0
50
100 μm
d
AFM surface height maps of dried lotus
50 μm
50 μm
50 μm
7 μm
0 μm
25
A
A
0
0
25
50 μm
Top scan
Section A-A
5
0
-5
Height (μm)
Top scan
+
Bottom scan
50 μm
50 μm
Bottom scan
Total
0
25
50 μm
e
PMMA low aspect ratio (LAR)
200 nm
1 μm
PMMA high aspect ratio (HAR)
200 nm
1 μm
f
Contact angle for various materials with varying surface structure
Contact angle (deg)
120
100
80
60
40
PMMA film
PMMA LAR
PMMA HAR
PFDTES on PMMA film
PFDTES on PMMA HAR

Table 1
Roughness parameters of microasperities (papillae) and nanobumps of hydrophobic leaves (dried and fresh lotus and colocasia) measured with AFM and optical profiler (based on Ref. [35])

Leaf	Scan size	State	Peak-valley height	Peak radius	Standard deviation of height σ (μm)	Correlation length β^* (μm)	Skewness	Kurtosis
Lotus	50 μm	Dried	9	4	1.1	4.8	2.0	6.7
	2 μm	Fresh	0.78	0.15	0.10	0.44	−0.36	3.3
		Dried	0.67	0.10	0.11	1.1	−0.41	3.4
Colocasia	50 μm	Dried	5	5	1.3	6.7	0.01	1.9
	2 μm bump	Fresh	0.53	0.07	0.09	0.24	0.11	2.5
		Dried	0.48	0.07	0.09	0.25	−0.11	2.6
	2 μm ridge	Fresh	0.68	0.12	0.10	0.48	−0.19	2.7
		Dried	0.57	0.11	0.08	0.31	−0.49	4.1

dependent with different characteristic scale lengths. To effectively resist these scale-dependent mechanisms, a multiscale (hierarchical) roughness is required. High asperities resist the capillary waves, while nanobumps prevent nanodroplets from filling the valleys between asperities and pin the triple line in case of a hydrophilic spot. Such multiscale roughness was found in natural and successful artificial superhydrophobic surfaces [17,19,20,23,26,27,31,33–35,38] (Fig. 4, Table 1). In the next section, we will consider scale effect on superhydrophobicity due to liquid pressure, which may be caused either by non-zero weight of a droplet or by pressure in the liquid flow.

2.5. Criteria for transition to the homogeneous interface

As it was stated above, a stable composite interface is essential for a successful design of superhydrophobic surfaces. However, the composite interface is fragile and it may irreversibly transform into the homogeneous interface. The mechanisms of this transition are subject of intensive investigation in recent years [9,11,13,14,16,22,23,38,40,41,48,49]. In the preceding section, we have studied destabilizing factors for the composite interface and found that the sign of the curvature is important, especially in the case of multiscale (hierarchical) roughness. We have also considered a stochastic approach for thermally activated transition between the metastable states. Among other factors, which affect the transition, the effects of droplet's weigh and curvature have been suggested.

The effect of droplet weight will be considered in detail in the following section for the case of patterned surfaces.

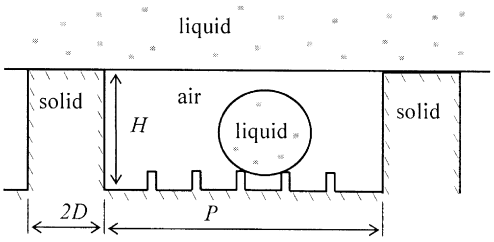

Fig. 5. Schematic of a rough surface with pillars. Smaller scale roughness is required to support small size droplets.

For small droplets, surface effects dominate over the gravity and the later is not responsible for the transition. Instead, the curvature of the droplet may be responsible. The curvature of a droplet is governed by the Laplace equation, which relates pressure inside the droplet to its curvature [3]. The curvature is the same at the top and the bottom of the droplet. However, a patterned surface with pillars of height H and pitch P, allows maximum droop in the cavity of about $P^2/8R$ [11,40,50]. When this droop exceeds the pillar height, the transition to the homogeneous interface may occur, therefore, ratio RH/P^2 controls the transition due to the droplet's curvature.

3. Wetting of patterned surfaces

In this section, we will consider patterned superhydrophobic surfaces with pillars. First, the effect of droplet weight and liquid pressure on the stability of the CI will be analyzed. Liquid pressure is created due to finite weight of a droplet or exists in the liquid flow, so these two cases will

Fig. 4. Experimental observations of superhydrophobic surfaces. (a) Scanning electron microscope (SEM micrographs of *Nelumbo nucifera* (*lotus*) leaf surface show hierarchical roughness with nanobumps (average peak-to-valley height 780 nm, mid-width 40 nm, peak radius 150 nm) on the top of microbumps (papillae, average peak-to-valley height 13 μm, mid-width 10 μm, peak radius 3 μm). (b) Nanobumps image obtained with atomic force microscopy (AFM), scan size 2 × 2 μm, microbumps measured using optical profiler. (c) Surface height map and a two-dimensional profile of a lotus leaf using an optical profiler [34]. (d) Surface height map and a two-dimensional profile of a lotus leaf (top tortion—top scan and bottom portion—bottom scan) using an AFM [34]. (e) SEM micrograph of the patterned poly(methyl methacrylate) (PMMA) surface. Both low aspect ratio (LAR, 1:1 height-to-diameter ratio) and high aspect ratio (HAR, 3:1 height-to-diameter ratio) asperities are shown from two magnifications to see the asperity shape and the asperity pattern on the surface [27]. (f) CA for different materials and for different roughness. CA decreased with increased roughness for the hydrophilic PMMA film. For a hydrophobic surface, the model predicts an increase of CA with roughness, which is what happens when PMMA HAR is coated with hydrophobic perfluorodecyltriethoxysilane (PFDTES) [27].

be considered here. Then, experimental observation will be discussed.

3.1. Effect of droplet weight

Consider a superhydrophobic surface with asperities or pillars with pitch P, diameter D and height H and density $\eta = 1/P$ asperities per area (Fig. 5). A droplet of radius R has weight of $\rho g 4/(3\pi R^3)$ which acts upon the composite interface area of $\pi(R\sin\theta)^2$, assuming that $\sin\theta$ is small, which is justified for a superhydrophobic surface. Thus, the pressure is

$$P_0 = \frac{4\rho g R}{3\sin^2\theta}. \tag{11}$$

It is convenient to introduce non-dimensional parameters, the spacing factor

$$S_f = \frac{D}{P}, \tag{12}$$

and normalized droplet radius

$$R_n = \frac{R}{P}. \tag{13}$$

Since the fractional solid–liquid area is given by $\eta\pi D^2/4$ or

$$f_{SL} = \frac{\pi S_f^2}{4}, \tag{14}$$

and since for the flat-top pillars $R_f = 1$, the CA and CAH can easily be presented as functions of S_f using Eqs. (4) and (5).

In the case of a composite interface, such a surface can support pressure given by the perimeter $\eta\pi D$, multiplied by $\sigma\cos\theta_0$, where σ is the surface tension, or

$$P_0 = \frac{\pi D\sigma\cos\theta_0}{P^2} = \frac{\pi\sigma S_f\cos\theta_0}{P}. \tag{15}$$

Comparing Eqs. (11) and (15) yields the condition for transition from the CI to HI due to the force of weight of the droplet

$$\frac{R_n}{S_f} = \frac{3\pi\sigma\sin^2\theta_0\cos\theta_0}{4\pi g}. \tag{16}$$

Thus, the relation of the gravity and surface forces is controlled by the ratio R_n/S_f. Note that, as it was stated above, the ratio R_nH/P controls the transition due to the droplet's curvature. Thus, we have identified three parameters, which control various modes of transition to the homogeneous interface: S_f is responsible for composite interface destabilization, R_n/S_f is responsible for the transition due to the gravity, and R_nH/P is responsible for the transition due to the droplet's curvature

3.2. Pressure in liquid flow

Liquid flow near rough walls, particularly, in microscopic channels, is an important application of superhydrophobic surfaces. As we have discussed in the preceding section, wetting behavior of solid surface with a liquid droplet is characterized by CA and CAH. For liquid flow applications, such as microfluidics, it is usually desirable to reduce the surface friction of liquid at a solid wall of a channel. The surface friction is characterized by a so-called slip length, l. Recent experimental observations and theoretical analyzes suggest that there is a correlation between wetting properties of a liquid and surface friction [30,51,52].

For continuous macroscale liquid flow near a solid surface, the boundary condition of no-slip (or zero flow velocity near wall) is normally assumed. It has been suggested recently, that liquid slip can exist over some surfaces due to a thin film of gas [51,52]. The slip is characterized by the so-called slip length or Navier length (Fig. 6), given by

$$l = H\left(\frac{\mu_L}{\mu_A} - 1\right), \tag{17}$$

where H is film thickness, μ_L and μ_A are viscosities of the liquid and air correspondingly [30].

Eq. (17) is valid for the case of pure liquid–air interface ($f_{SL} = 0$). For a more realistic case of a composite interface, we will assume that that average slip length is given by averaging over the area of the slip length at the liquid–air interface (fractional area of $1-f_{SL}$), given by Eq. (17) and zero slip velocity at the solid–liquid interface (fractional area of f_{SL})

$$l = H\left(\frac{\mu_L}{\mu_A} - 1\right)(1 - f_{SL}). \tag{18}$$

Whereas for a pure composite interface, f_{SL} can be calculated from Eq. (14), for a mixed interface f_{SL} can be calculated using probabilities of liquid filling a valley or air pocket staying there.

The thickness of the layer H is assumed to be equal to the pillars height. Based on Eq. (18), the higher the pillars, the larger is the slip length and, therefore, smaller is resistance to liquid flow. Note that maximum pressure, which can be supported by the surface, is still given by Eq. (15). Stability of the composite interface, discussed in the preceding sections, still remains an important issue.

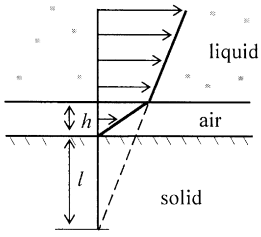

Fig. 6. Slip length and velocity distribution in a liquid flow over a gas film near a solid wall. Since gas viscosity is much smaller than that of the liquid, the observed slip length l has a finite value given by Eq. (18).

3.3. Experimental observations

Bhushan et al. [49] studied wetting of two series of nine samples of single-crystal silicon (Si), coated with hydrophobic 1,1,-2,2,-tetrahydroperfluorodecyltrichlorosilane (PF_3) self-assembled monolayer. Series 1 has 5-μm diameter and 10-μm height flat-top, cylindrical pillars with different pitch values (7, 7.5, 10, 12.5, 25, 37.5, 45, 60, and 75 μm), and Series 2 has 14-μm diameter and 30-μm height flat-top, cylindrical pillars with different pitch values (21, 23, 26, 35, 70, 105, 126, 168, and 210 μm). The flat Si coated with PF_3 showed the advancing CA of 116°, the receding CA of 82°, CAH of 34°.

Their experimental data for CA and CAH are in good agreement with Eqs. (4) and (5) (Fig. 7). Furthermore, the experimental values of the CA and CAH depend only upon the non-dimensional spacing factor and not upon actual size of the pillars. As the spacing factor decreases up to $S_f = 0.11$ (the pitch of 45 μm in Series 1 and 126 μm of Series 2), the CA increases gradually from 152° to 170° (Fig. 7a). Then, the CA starts decreasing sharply, indicating for a transition from the composite to homogeneous interface. The non-dimensional droplet size at the point before the transition was equal to $\eta = 23.6$ and 7.3. It is noted that the transition takes place at the critical value of $0.083 < S_f < 0.111$. This suggests that the spacing factor and the fractional solid–liquid area of contact (which is directly related to S_f according to Eq. (14)) are responsible for the transition.

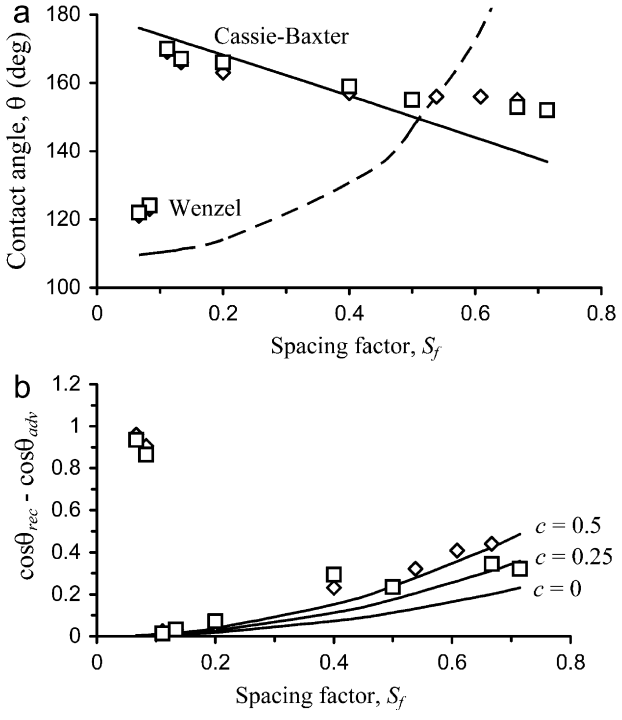

Fig. 7. (a) Static CA θ as a function of the spacing factor S_f for the first (squares) and the second (diamonds) series of the experiments compared with the Wenzel and Cassie–Baxter models. (b) The values of $\cos\theta_{rec} - \cos\theta_{adv}$ as a function of S_f for the first (squares) and the second (diamonds) series of the experiments compared with the theoretically predicted values (solid line).

The values of the CA are plotted against the theoretically predicted value, based on the Wenzel (calculated using Eq. (2), $R_f = 1 + \pi HD/P^2$) and Cassie–Baxter (calculated using Eq. (4)) models, whereas the values of CAH $\cos\theta_{rec} - \cos\theta_{adv}$ are plotted against the theoretically predicted value given by Eq. (5)with $H_r = cS_f^2$, $c = 0$, 0.25, 0.5 (Fig. 7b). The lowest CAH of 5° was observed at $S_f = 0.111$. There is a good agreement between the experimental data and the theoretically predicted values for $c = 0.5$. It is noted, that the theoretically predicted values for $c = 0$ (no effect of the surface roughness) underestimate CAH, with the experimental values approximately twice larger. This result suggests that the contact area and adhesion hysteresis gives approximately the same contribution into the CAH as the roughness and sharp edges. It is concluded from the analysis of the theoretical data, that the spacing factor is the most important parameter for design and optimization of patterned superhydrophobic surfaces.

4. Roughness optimization for superhydrophobicity and liquid flow

In the preceding sections, we considered theoretical and experimental superhydrophobic surfaces and liquid flow near rough surface walls and found that roughness can enhance hydrophobicity and decrease resistance to the flow, however, there are several factors which control this effect, and these factors are scale-dependent. Furthermore, natural superhydrophobic surfaces also exhibit hierarchical roughness structure. Therefore, a successful water-repellent surface should also have multiscale roughness. In this section, we are looking for optimization conditions of optimized biomimetic water-repellent surfaces. Optimization is a combination of confliction requirements, so we will formulate these requirements first.

Water-repellent surfaces should have

- *High CA*: To achieve high CA, based on Eqs. (4) and (15), either high R_f or low S_f are required.
- *Low CAH*: To achieve low CAH, based on Eqs. (5) and (14), low R_f and S_f, and stable composite interface are required. Thus, based on this and preceding requirement, composite interface is necessary.
- *High slip length*, for which maximum height of asperities (or pillars) H is required, based on Eq. (18).
- Ability to support high liquid pressure requires high spacing factor S_f and large perimeter (or diameter) of pillars, based on Eq. (15).
- Ability to support wide range of droplet sizes requires hierarchical roughness with a certain spacing factor.

Stability of the composite interface implies ability to resist destabilizing factors, i.e., interface capillary waves, condensation of nanodroplets and surface inhomogeneity

as well as liquid pressure. To resist capillary waves, high asperities are required. To resist nanoscale droplets, hierarchical roughness is required, and to resist surface inhomogeneity nanobumps should be convex for stability of the liquid–air interface, as discussed above. In addition, the surface should be initially hydrophobic, that is $\theta_0 > \pi/2$. Height of asperities is limited by their structural strength, and it is well known from mechanical consideration, that maximum height-to-width ratio required to support strength increases with decreasing scale. The requirement of low f_{SL} and high η and p are conflicting, to order to combine them, the pillars should be at least dense and wide enough to provide with the spacing factor given by Eq. (12).

We finally come with the following set of requirements for optimized roughness distribution:

1. Roughness should be hierarchical, with several scale sizes, from microbumps to nanobumps. Largest asperities should be small compared to maximum droplet size, given by the capillary length.
2. Asperities should be high with their height limited by the requirement of their structural strength. It is known that the strength of geometrically similar structures increases with decreasing scale, since forces (e.g., weight) are usually proportional to volume and therefore the third power of length, while strength is proportional to the cross-section area and thus to the second power of length.
3. Asperities at each scale level should have small-width and large distance between them (small S_f), however, this requirement is limited by some critical value of the spacing factor, providing the ability to support required pressure. The critical value found experimentally by Bhushan et al. [49] was in the range $0.083 < S_f < 0.111$. For liquid flow, a compromise between ability to support pressure and the slip length is required. In addition, large pitch between asperities may lead to destabilization due to the capillary waves.
4. Nanoasperities should be convex (bumps rather than grooves) to stabilize the liquid–air interface.
5. For initially hydrophilic surface, a hydrophobic coating is required.

Table 2
Roughness optimization for superhydrophobic surfaces

Purpose	Method to achieve	Problems	Solution
High CA	Composite interface (low S_f)	Condensation of nanodroplets	Hierarchical roughness
Low CAH		Surface inhomogeneity	Convex asperities
High slip length		Liquid-air interface waves	High asperities, but not exceeding structural strength limit
	High asperities	Exceeding maximum structural strength	
Support high pressure	High density and perimeter of asperities	Contradicts to low S_f	Not to exceed required spacing factor
Support both micro- and nanodroplets	Hierarchical roughness		

These requirements for a rough surface are summarized in Table 2. Remarkably, all these requirements are satisfied by biological water-repellent surfaces, such as leaves, which have hierarchical roughness with tightly packed convex papillae (asperities) and nanobumps/nano-"hairs" above them as well as hydrophobic wax coating (Fig. 4, Table 1).

5. Conclusions

We have investigated design requirements for artificial roughness-induced superhydrophobic surfaces. These surfaces should provide with high CAs, CAH and high slip lengths, and be able to support liquid pressure, created either by liquid flow or liquid droplet weight. To satisfy these requirements, a composite solid–liquid–air interface should be formed. In order for the composite interface to be stable and not to be destroyed due to capillary liquid–air interface waves, condensation of nanodroplets and local hydrophilic spots due to surface chemical inhomogeneity, roughness should be hierarchical with nanoasperities over microasperities. Convex ("bumpy") nanoasperities can pin the liquid–air interface and thus prevent liquid from filling the valleys between asperities. Nanoroughness is required also to support nanodroplets, which may condensate in the valleys between large asperities. Both the condition of supporting the nanodroplets and condition of structural strength of the pillars result in smaller asperities having much higher height-to-thickness ratio (aspect ratio), which is controlled by the asperities spacing factor, given by Eq. (12). Based on these considerations, we formulated the set of five requirements for roughness distribution and showed that natural superhydrophobic surfaces follow these requirements.

References

[1] B. Bhushan, Nanotribology and Nanomechanics—An Introduction, Springer, Heidelberg, Germany, 2005.
[2] B. Bhushan, Springer Handbook of Nanotechnology, second ed., Springer, Heidelberg, Germany, 2006.
[3] A.V. Adamson, Physical Chemistry of Surfaces, Wiley, New York, 1990.
[4] J.N. Israelachvili, Intermolecular and Surface Forces, second ed., Academic Press, London, 1992.
[5] R.N. Wenzel, Ind. Eng. Chem. 28 (1936) 988.
[6] A. Cassie, S. Baxter, Trans. Faraday Soc. 40 (1944) 546.
[7] R.E. Johnson, R.H. Dettre, Contact angle hysteresis, contact angle, wettability, and adhesion, in: F.M. Fowkes (Ed.), Advanced Chemical Series, 43, American Chemical Society, Washington, DC, 1964, pp. 112–135.
[8] J. Bico, U. Thiele, D. Quéré, Colloids Surf. A 206 (2002) 41.

[9] A. Marmur, Langmuir 19 (2003) 8343.
[10] A. Marmur, Langmuir 20 (2004) 3517.
[11] A. Lafuma, D. Quėrė, Nat. Mater. 2 (2003) 457.
[12] N.A. Patankar, Langmuir 19 (2003) 1249.
[13] N.A. Patankar, Langmuir 20 (2004) 7097.
[14] B. He, N.A. Patankar, J. Lee, Langmuir 19 (2003) 4999.
[15] W. Li, A. Amirfazli, J. Colloid Interface Sci. 292 (2006) 195.
[16] C.W. Extrand, Langmuir 18 (2002) 7991.
[17] S. Herminghaus, Europhys. Lett. 52 (2000) 165.
[18] N.A. Patankar, Langmuir 20 (2004) 8209.
[19] M. Sun, C. Luo, L. Xu, H. Ji, Q. Ouyang, D. Yu, Y. Chen, Langmuir 21 (2005) 8978.
[20] S. Shibuichi, T. Onda, N. Satoh, K. Tsujii, J. Phys. Chem. 100 (1996) 19512.
[21] M. Nosonovsky, B. Bhushan, Microsyst. Technol. 11 (2005) 535.
[22] M. Nosonovsky, B. Bhushan, Microsyst. Technol. 12 (2006) 231.
[23] M. Nosonovsky, B. Bhushan, Microsyst. Technol. 12 (2006) 273.
[24] F.G. Yost, J.R. Michael, E.T. Eisenmann, Acta Metall. Mater. 45 (1995) 299.
[25] S. Semal, T.D. Blake, V. Geskin, M.L. de Ruijter, G. Castelein, J. De Coninck, Langmuir 15 (1999) 8765.
[26] H.Y. Erbil, A.L. Demirel, Y. Avci, Science 299 (2003) 1377.
[27] Z. Burton, B. Bhushan, Nano. Lett. 5 (2005) 1607.
[28] F. Porcheron, P.A. Monson, Langmuir 22 (2006) 1595.
[29] J. Zhang, D.Y. Kwok, Langmuir 22 (2006) 4998.
[30] C.-H. Choi, C.-J. Kim, Phys. Rev. Lett. 96 (2006) 066001.
[31] C. Neinhuis, W. Barthlott, Ann. Bot. 79 (1997) 667.
[32] P. Wagner, R. Furstner, W. Barthlott, C. Neinhuis, J. Exp. Bot. 54 (385) (2003) 1295.
[33] X.F. Gao, L. Jiang, Nature 432 (2004) 36.
[34] Z. Burton, B. Bhushan, Ultramicroscopy 106 (2006) 709.
[35] B. Bhushan, Y.C. Jung, Nanotechnology 17 (2006) 2758.
[36] T. Onda, S. Shibuichi, N. Satoh, K. Tsujii, Langmuir 12 (1996) 2125.
[37] Y.T. Cheng, D.E. Rodak, A. Angelopoulos, T. Gacek, Appl. Phys. Lett. 87 (2005) 194112.
[38] M. Miwa, A. Nakajima, A. Fujishima, K. Hashimoto, T. Watanabe, Langmuir 16 (2000) 5754.
[39] J. Kijlstra, K. Reihs, A. Klami, Colloids Surf. A: Physicochem. Eng. Aspects 206 (2002) 521.
[40] M. Nosonovsky, B. Bhushan, in: B. Bhushan (Ed.), Applied Scanning Probe Methods, 5, Springer, 2007, pp. 1–40.
[41] M. Nosonovsky, B. Bhushan, Microelectron. Eng. 84 (2007) 382.
[42] D. Quéré, Nat. Mater. 3 (2004) 79.
[43] A. Checco, P. Guenoun, J. Daillant, Phys. Rev. Lett. 91 (2003) 186101.
[44] P.S. Swain, R. Lipowsky, Langmuir 14 (1998) 6772.
[45] S Zinger, private communication, Ohio State University, 2004.
[46] H. Kamusewitz, W. Possart, D. Paul, Colloids Surf. A 156 (1999) 271.
[47] Y.T. Cheng, D.E. Rodak, C.A. Wong, C.A. Hayden, Nanotechnology 17 (2006) 1359.
[48] K.A. Wier, T.J. McCarthy, Langmuir 22 (2006) 2433.
[49] B. Bhushan, M. Nosonovsky, Y.C. Jung. J. R. Soc. Interface (2007, in press, doi:10.1098/rsif.2006.0211).
[50] M. Reyssat, D. Quere, personal communications, 2006.
[51] P.G. de Gennes, Langmuir 18 (2002) 3413.
[52] C. Cottin-Bizonne, J.-L. Barrat, L. Bocquet, E. Charlaix, Nat. Mater. 2 (2003) 237.